

Interaction-driven spin precession in quantum-dot spin valves

Jürgen König¹ and Jan Martinek^{1,2}

¹*Institut für Theoretische Festkörperphysik, Universität Karlsruhe, 76128 Karlsruhe, Germany*

²*Institute of Molecular Physics, Polish Academy of Sciences, 60-179 Poznań, Poland*

(Dated: May 21, 2019)

We analyze spin-dependent transport through spin valves composed of an interacting quantum dot coupled to two ferromagnetic leads. The spin on the quantum dot and the linear conductance as a function of the relative angle θ of the leads' magnetization directions is derived to lowest order in the dot-lead coupling strength. Due to the applied bias voltage spin accumulates on the quantum dot, which for finite charging energy experiences a torque, resulting in spin precession. The latter leads to a non-trivial, interaction-dependent, θ -dependence of the conductance. In particular, we find that the spin-valve effect is reduced for all $\theta \neq \pi$.

PACS numbers: 72.25.Mk, 73.63.Kv, 85.75.-d, 73.23.Hk

Introduction. – The field of spin- or magnetoelectronics has attracted much interest, for both its beautiful fundamental physics and its potential applications. One famous spin-dependent transport phenomenon is the tunnel magnetoresistance (TMR) in a *spin-valve* geometry, in which two ferromagnetic metals are separated by an insulating layer serving as a tunnel barrier [1]. The transmission through the barrier decreases as the relative angle θ between the magnetizations of two ferromagnets is increased from 0 to π . Within a single-particle picture the θ -dependent part of the transmission can be shown [2, 3] to be proportional to $\cos \theta$.

Tunneling based on tunneling has also been extensively studied in nanostructured devices such as semiconductor quantum dots (QDs) or metallic single-electron transistors. Recently, magnetotransport through those devices has attracted much interest. This includes normal or ferromagnetic metallic islands coupled to ferromagnetic leads [4, 5] as well as spin-dependent transport from ferromagnets through QDs [6, 7]. Precession of a single magnetic atom spin in an external magnetic field has been detected, but only in the power spectrum of the tunneling current [8, 9].

In this Letter, we study the effect of strong Coulomb interaction in a single-level QD (or a magnetic impurity [10]) attached to ferromagnetic leads on the average dot spin and the linear conductance in the weak dot-lead coupling limit. We find an interaction-driven spin precession, even in the absence of an external magnetic field. This spin precession is predicted to be clearly visible in the linear conductance as a reduction of the spin-valve effect and a nontrivial θ -dependence. For any non-parallel configuration, transport is reduced as compared to the parallel one (spin-valve effect). In the absence of Coulomb interaction, the θ -dependence follows simply $\cos \theta$ [2, 3]. The presence of a finite charging energy, however, leads to a reduction of the spin-valve effect. This can be understood by the interplay of spin accumulation caused by the bias voltage and an interaction-dependent spin torque due to an effective exchange interaction between

the spin in the dot and the leads, which in turn generates spin precession, detectable in the conductance.

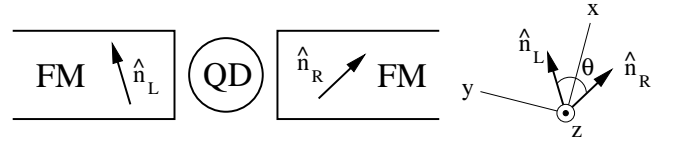


FIG. 1: A quantum-dot spin valve. A quantum dot (QD) is connected to two ferromagnetic leads (FM). The coordinate system we use is shown on the right. The magnetization directions (arrows) enclose an angle θ .

The model. – We consider a small QD with one spin-degenerate energy level ϵ participating in transport. The left and right lead are magnetized along $\hat{\mathbf{n}}_L$ and $\hat{\mathbf{n}}_R$, respectively (see Fig. 1), with the relative angle θ . The total Hamiltonian is the sum of five parts, $H = H_{\text{dot}} + H_L + H_R + H_{T,L} + H_{T,R}$. The first one, $H_{\text{dot}} = \epsilon \sum_{\sigma} c_{\sigma}^{\dagger} c_{\sigma} + U n_{\uparrow} n_{\downarrow}$, describes the dot energy level plus the charging energy U for double occupation of the dot. The next two model the leads, $H_r = \sum_k \epsilon_k a_{rk}^{\dagger} a_{rk}$, with $r = L, R$. For simplicity, we assume the leads to be half metallic, i.e., only majority spins have a finite density of states. Tunneling between lead and dot is described by $H_{T,L} = t \sum_k (a_{Lk}^{\dagger} c_{+} + h.c.)$, where c_{+} is the Fermi operator for an electron on the QD with spin along the direction of the magnetization of the left lead. It is convenient to use the coordinate system defined by $\hat{\mathbf{e}}_x = (\hat{\mathbf{n}}_L + \hat{\mathbf{n}}_R)/|\hat{\mathbf{n}}_L + \hat{\mathbf{n}}_R|$, $\hat{\mathbf{e}}_y = (\hat{\mathbf{n}}_L - \hat{\mathbf{n}}_R)/|\hat{\mathbf{n}}_L - \hat{\mathbf{n}}_R|$, and $\hat{\mathbf{e}}_z = (\hat{\mathbf{n}}_R \times \hat{\mathbf{n}}_L)/|\hat{\mathbf{n}}_R \times \hat{\mathbf{n}}_L|$, and to quantize the dot spin along the z -direction. In this basis, the tunnel Hamiltonian reads

$$H_{T,L} = \frac{t}{\sqrt{2}} \sum_k \left(e^{i\theta/4} a_{Lk}^{\dagger} c_{\uparrow} + e^{-i\theta/4} a_{Lk}^{\dagger} c_{\downarrow} + h.c. \right), \quad (1)$$

and $H_{T,R}$ is the same but with $L \rightarrow R$ and $\theta \rightarrow -\theta$. Due to tunneling the dot level acquires a finite width $\Gamma = 2\pi|t|^2 N$, where $N = N_L = N_R$ is the density of states of the majority spins of the left and right lead.

With this particular choice of the quantization axis, the model studied here appears similar to those for Aharonov-Bohm interferometers which contain a single-level QD in each arm [11, 12, 13]. In the present case, the two “arms” are labeled by the spin $\sigma = \uparrow, \downarrow$ along the z -direction, and the Aharonov-Bohm phase due to an enclosed magnetic flux corresponds to the angle θ between the leads’ magnetizations. The limit $U \rightarrow \infty$ of the present model is, in fact, equivalent to the one studied in Sec. IV. C. of Ref. 12.

Linear conductance and average spin. – We make use of the analogy between the quantum-dot spin valve and the Aharonov-Bohm interferometer and express the current in terms of Green’s functions of the dot electrons, as shown in Eq. (4.3) of Ref. 12. Here, we are interested in first-order transport in Γ , for which the linear-response conductance $G^{\text{lin}} = (\partial I / \partial V)|_{V=0}$ simplifies to [15]

$$G^{\text{lin}} = \frac{2e^2}{h} \Gamma \int d\omega \left\{ \text{Im } G_{\downarrow\downarrow}^{\text{ret}}(\omega) f'(\omega) + \sin \frac{\theta}{2} f(\omega) \frac{\partial G_{\downarrow\uparrow}^>(\omega)}{\partial(eV)} + \sin \frac{\theta}{2} [1 - f(\omega)] \frac{\partial G_{\downarrow\uparrow}^<(\omega)}{\partial(eV)} \right\}. \quad (2)$$

Here, $f(\omega)$ is the Fermi function, $G_{\sigma\sigma'}(\omega)$ are the Fourier transforms of the Green’s functions $G_{\sigma\sigma'}^>(t) = -i\langle c_\sigma(t)c_{\sigma'}^\dagger(0) \rangle$, $G_{\sigma\sigma'}^<(t) = i\langle c_{\sigma'}^\dagger(0)c_\sigma(t) \rangle$, and $G_{\sigma\sigma'}^{\text{ret}}$ is the usual retarded Green’s function. Contributions involving $\text{Im } G_{\uparrow\uparrow}^{\text{ret}}(\omega)$, $G_{\uparrow\downarrow}^>(\omega)$, and $G_{\uparrow\downarrow}^<(\omega)$ are accounted for in the prefactor 2. Since Γ already appears explicitly in front of the integral, all Green’s functions are to be taken to zeroth order in Γ . In this limit, we find $-(1/\pi)\text{Im } G_{\downarrow\downarrow}^{\text{ret}}(\omega) = (P_0^\uparrow + P_\downarrow^\downarrow)\delta(\omega - \epsilon) + (P_\uparrow^\uparrow + P_d^\downarrow)\delta(\omega - \epsilon - U)$, $G_{\downarrow\uparrow}^{\text{ret}}(\omega) = 2\pi i P_\uparrow^\downarrow \delta(\omega - \epsilon - U)$, and $G_{\downarrow\uparrow}^<(\omega) = 2\pi i P_\uparrow^\downarrow \delta(\omega - \epsilon)$, where $P_\chi^x = \langle |\chi^x\rangle \langle \chi| \rangle$ are elements of the stationary density matrix (to zeroth order in Γ) of the quantum dot subsystem, with $\chi, \chi' = 0$ (empty dot), \uparrow, \downarrow (singly-occupied dot), and d (doubly-occupied dot).

The main task is now to determine these density matrix elements to zeroth order in Γ . They contain as well the information about the average occupation and spin on the QD. The diagonal matrix elements, P_χ^x , are nothing but the probabilities to find the QD in state χ , i.e., the dot is empty with probability P_0^\uparrow , singly occupied with $P_1 \equiv P_\uparrow^\uparrow + P_\downarrow^\downarrow$, and doubly occupied with P_d^\downarrow . A finite spin can only emerge for single occupancy. The average spin $\mathbf{S} = (S_x, S_y, S_z)$ is related to the off-diagonal matrix element P_\uparrow^\downarrow via $S_x = \text{Re } P_\uparrow^\downarrow$, $S_y = \text{Im } P_\uparrow^\downarrow$, and $S_z = (1/2)(P_\uparrow^\uparrow - P_\downarrow^\downarrow)$.

It is remarkable that on the r.h.s of Eq. (2) derivatives of Green’s function with respect to bias voltage V appear. As a consequence, not only the equilibrium density matrix elements enter the linear conductance, but

also linear corrections in V are involved. In equilibrium, $V = 0$, the density matrix is diagonal with $P_0^\uparrow = 1/Z$, $P_\uparrow^\uparrow = P_\downarrow^\downarrow = \exp(-\beta\epsilon)/Z$, $P_d^\downarrow = \exp[-\beta(2\epsilon + U)]/Z$, with $Z = 1 + 2\exp(-\beta\epsilon) + \exp[-\beta(2\epsilon + U)]$ and $\beta = 1/(k_B T)$. As a consequence, the average spin on the QD vanishes at $V = 0$ [16]. With applied bias voltage, though, a finite spin can accumulate, which yields a finite $(d\mathbf{S}/dV)|_{V=0}$.

We now determine the needed density matrix elements by using the real-time transport theory developed in Ref. 14. The starting point is the generalized stationary master equation in Liouville space,

$$(\epsilon_{\chi_1} - \epsilon_{\chi_2}) P_{\chi_2}^{\chi_1} + \sum_{\chi'_1, \chi'_2} P_{\chi'_2}^{\chi'_1} \Sigma_{\chi'_2, \chi_2}^{\chi'_1, \chi_1} = 0, \quad (3)$$

where χ_1 and χ_2 label the QD states, and ϵ_{χ_1} and ϵ_{χ_2} are the corresponding energies. The matrix elements $P_{\chi_2}^{\chi_1}$ of the density matrix are connected to each other in Eq. (3) by terms $\Sigma_{\chi'_2, \chi_2}^{\chi'_1, \chi_1}$ which can be viewed as generalized transition rates in Liouville space. They are defined as irreducible self-energy parts of the propagation in Liouville space and are represented as diagram blocks on a Keldysh contour. For a detailed derivation of this diagrammatic language, the generalized master equation, and the rules on how to calculate a diagram we refer to Ref. 14.

In the following, we write $P = \bar{P} + \hat{P} + \dots$ and $\Sigma = \bar{\Sigma} + \hat{\Sigma} + \dots$, where \bar{P} and $\bar{\Sigma}$ denote the equilibrium limit, and \hat{P} and $\hat{\Sigma}$ are the linear corrections in V . Using the symmetry of the model, we find the relations $\bar{P}_\chi^{\chi'} = \bar{P}_{\bar{\chi}}^{\bar{\chi}'}$ and $\bar{\Sigma}_{\chi, \chi''}^{\chi', \chi'''} = \bar{\Sigma}_{\bar{\chi}, \bar{\chi}''}^{\bar{\chi}', \bar{\chi}'''}$ and $\hat{P}_\chi^{\chi'} = -\hat{P}_{\bar{\chi}}^{\bar{\chi}'}$ and $\hat{\Sigma}_{\chi, \chi''}^{\chi', \chi'''} = -\hat{\Sigma}_{\bar{\chi}, \bar{\chi}''}^{\bar{\chi}', \bar{\chi}'''}$, where $\bar{\chi}$ is obtained from χ by the transformation $\uparrow \leftrightarrow \downarrow$. For transitions from diagonal states in Liouville space to diagonal ones we find $\hat{\Sigma}_{\chi, \chi'}^{\chi, \chi'} = 0$. Finally, we drop all Σ terms which connect states in Liouville space that are not compatible, at least to lowest order in Γ . It turns out that it is sufficient to specify Eq. (3) for $\chi_1 = \chi_2 = \downarrow$ as well as for $\chi_1 = \downarrow, \chi_2 = \uparrow$. For the linear correction in V we get

$$\begin{aligned} 0 &= \hat{P}_\downarrow^\downarrow \bar{\Sigma}_{\downarrow, \downarrow}^{\downarrow, \downarrow} + \hat{P}_\uparrow^\downarrow \left(\bar{\Sigma}_{\uparrow, \downarrow}^{\downarrow, \downarrow} - \bar{\Sigma}_{\downarrow, \uparrow}^{\downarrow, \downarrow} \right) \\ 0 &= \hat{P}_\uparrow^\downarrow \bar{\Sigma}_{\uparrow, \uparrow}^{\downarrow, \downarrow} + \hat{P}_\downarrow^\downarrow \left(\bar{\Sigma}_{\downarrow, \uparrow}^{\downarrow, \downarrow} - \bar{\Sigma}_{\uparrow, \uparrow}^{\downarrow, \downarrow} \right) \\ &\quad + \bar{P}_0^\uparrow \hat{\Sigma}_{0, \uparrow}^{0, \downarrow} + \bar{P}_\downarrow^\downarrow \left(\hat{\Sigma}_{\downarrow, \uparrow}^{\downarrow, \downarrow} + \hat{\Sigma}_{\uparrow, \uparrow}^{\downarrow, \downarrow} \right) + \bar{P}_d^\downarrow \hat{\Sigma}_{d, \uparrow}^{d, \downarrow}. \end{aligned} \quad (4)$$

We evaluate the all necessary diagrams $\Sigma_{\chi'_2, \chi_2}^{\chi'_1, \chi_1}$ explicitly. Eventually, we find the solution

$$\hat{P}_\uparrow^\downarrow = \frac{i}{4} \frac{eV}{k_B T} \bar{P}_1 \cos^2 \alpha(\theta) \sin \frac{\theta}{2} \quad (6)$$

and $\hat{P}_\downarrow^\downarrow = -\hat{P}_\uparrow^\downarrow = i \hat{P}_\uparrow^\downarrow \tan \alpha(\theta)$. We used the definition

$$\tan \alpha(\theta) = \frac{A}{1 - f(\epsilon) + f(\epsilon + U)} \cos \frac{\theta}{2}, \quad (7)$$

where $A = \frac{1}{\pi} \text{Re} \left[\Psi \left(\frac{1}{2} + i \frac{\beta \epsilon}{2\pi} \right) - \Psi \left(\frac{1}{2} + i \frac{\beta(\epsilon+U)}{2\pi} \right) \right]$, and $\Psi(x)$ denotes the digamma function. This means that the spin accumulated in the QD is (for $eV \ll k_B T$)

$$|\mathbf{S}| = \sqrt{S_y^2 + S_z^2} = \frac{eV}{4k_B T} \bar{P}_1 \cos \alpha(\theta) \sin \frac{\theta}{2}, \quad (8)$$

with $\alpha(\theta)$ being the angle enclosed by the quantum-dot spin and the y -axis, $\tan \alpha(\theta) = S_z/S_y$.

With the result for $\hat{P}_\uparrow^\downarrow$ we are able to obtain the linear conductance. It can be written in the compact form

$$G^{\text{lin}} = G^{\text{lin},\text{max}} \left(1 - \cos^2 \alpha(\theta) \sin^2 \frac{\theta}{2} \right). \quad (9)$$

This equation together with the condition for $\alpha(\theta)$, Eq. (7), is the central result of this paper. The conductance is maximal for parallel magnetization, $\theta = 0$. Its value is $G^{\text{lin},\text{max}} = (2\pi e^2/h)(\Gamma/k_B T)[1-f(\epsilon+U)]f(\epsilon)[1-f(\epsilon)+f(\epsilon+U)]/[f(\epsilon)+1-f(\epsilon+U)]$.

We can straightforwardly generalize our theory to allow for arbitrary spin polarization $p \equiv (N_{\text{maj}} - N_{\text{min}})/(N_{\text{maj}} + N_{\text{min}})$ in the leads. In this case, we get $G^{\text{lin}}/G^{\text{lin},\text{max}} = 1 - p^2 \cos^2 \alpha_p(\theta) \sin^2(\theta/2)$ with $\tan \alpha_p(\theta) = p \tan \alpha_{p=1}(\theta)$.

Results and discussion. – It is interesting to analyze how Coulomb interaction in the dot affects the spin accumulation in our model. In the absence of charging energy, $U = 0$, we find $A = 0$ and $\alpha = 0$, and the accumulated spin is along the y -direction, i.e., along $\hat{\mathbf{n}}_L - \hat{\mathbf{n}}_R$. A finite charging energy, however, yields a rotation of the quantum-dot spin within the $y-z$ -plane by an angle α , accompanied by a reduction of the total accumulated spin by $\cos \alpha$. The origin of the torque responsible for this spin rotation is an interaction-dependent effective spin exchange of the quantum-dot spin with the lead spins. In the subspace of single dot occupation an effective spin Hamiltonian can be derived from the full model by means of a Schrieffer-Wolff transformation. If we now employ a mean-field picture and replace the lead spin operators by their average value, we end up with the simple effective Hamiltonian $H^{\text{eff}} = A\Gamma \cos(\theta/2)S_x$ for the subspace under consideration. In this effective model, a spin in the $y-z$ -plane experiences a torque and starts to precess, as described by classical Bloch equations. Together with the rate $\Gamma_{1 \rightarrow 0} + \Gamma_{1 \rightarrow d} = \Gamma[1-f(\epsilon)+f(\epsilon+U)]$ to diminish the z -component of the quantum-dot spin by changing the dot state from single occupation to an empty or doubly-occupied dot via tunneling, we get the Bloch equation $dS_z/dt = A\Gamma \cos(\theta/2)S_y - (\Gamma_{1 \rightarrow 0} + \Gamma_{1 \rightarrow d})S_z$, from which we can extract the angle $\alpha(\theta)$ of the rotated spin in the stationary limit $dS_z/dt = 0$, and we recover Eq. (7).

We emphasize that both the rates for changing the number of dot electrons and the spin precession are of the same order in Γ , which is why the angle α is Γ -independent. The two types of processes correspond to two different kinds of diagrams $\Sigma_{\chi_2, \chi_2}^{\chi_1, \chi_1}$. In spin-precession

terms, all four labels $\chi_1, \chi_1', \chi_2', \chi_2$ represent single occupation, \uparrow, \downarrow . They describe first-order virtual charge fluctuations during which the spin is rotated. In contrast, tunneling rates which change the number of dot electrons are described by diagrams with $\chi_1 = \chi_1' = 0$ or $\chi_1 = \chi_1' = d$ or $\chi_2 = \chi_2' = 0$, or $\chi_2 = \chi_2' = d$. It is crucial for a consistent theory of first-order transport to include both types of diagrams in the master equations (4) and (5).

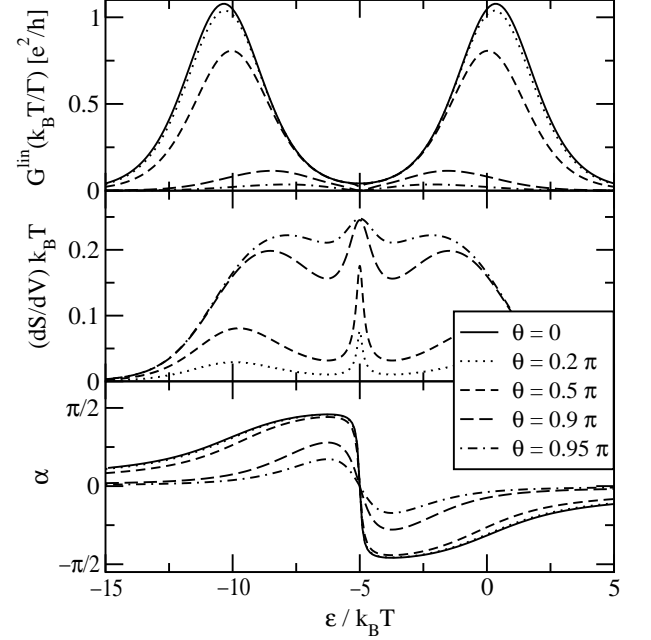


FIG. 2: Upper panel: Linear conductance (normalized by $\Gamma/k_B T$ and plotted in units of e^2/h) as a function of level position ϵ for five different angles θ . Middle panel: Derivative of accumulated spin S with respect to bias voltage V normalized by $k_B T$. Lower panel: angle α between the quantum-dot spin and the y -axis. In all panels we have chosen the charging energy $U = 10k_B T$ and half-metallic leads.

The linear conductance as a function of the level energy ϵ is plotted in the upper panel of Fig. 2 for interaction strength $U = 10k_B T$ and different values of the angle θ . For parallel magnetization, $\theta = 0$, there are two conductance peaks located near $\epsilon = 0$ and $\epsilon = -U$, respectively. With increasing angle θ , transport is more and more suppressed due to the spin-valve effect. However, this suppression is not uniform, as would be in the absence of charging energy. In contrast, the spin-valve effect is less pronounced in the valley between the two peaks, where the dot is dominantly singly occupied, and spin accumulation can occur. As a consequence, the two peaks move towards each other with increasing θ .

The differential spin accumulation dS/dV in units of $k_B T$ is illustrated in the middle panel of Fig. 2. It is clear that single occupation of the dot is required for spin accumulation, i.e., the plotted signal is high in the valley between the two conductance peaks.

As explained above, an effective exchange interaction between quantum-dot spin and spin of the leads yield a rotation of the accumulated spin in the $y-z$ -plane by an angle α . The lower panel of Fig. 2 depicts the evolution of α as a function of the level energy ϵ . This angle is large in the valley between the conductance peaks, getting close to $\pm\pi/2$. A special point is $\epsilon = -U/2$, at which, due to particle-hole symmetry, the effective exchange interaction vanishes. As a consequence, α shows a sharp transition from positive to negative values, accompanied with a peak in the accumulated spin.

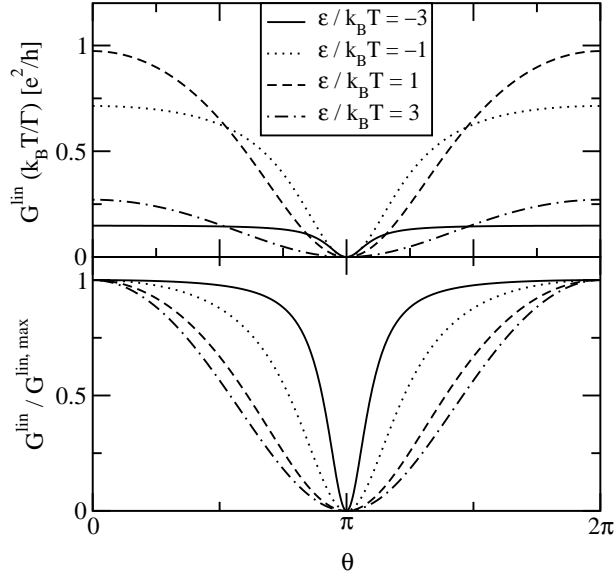


FIG. 3: Upper panel: Linear conductance as a function of θ for $U = 10k_B T$ and four different values of the level position. Lower panel: The same but normalized to the maximal conductance for parallel magnetization.

In the upper panel of Fig. 3 we show the linear conductance as a function of θ for four values of ϵ . For $\epsilon/k_B T = 3$ and 1, the dot is predominantly empty, and the θ -dependence of the conductance is almost harmonic. For $\epsilon/k_B T = -1$ and -3 , however, the spin-valve effect is strongly reduced, and conductance is enhanced, except in the regime close to antiparallel magnetization, $\theta = \pi$. The enhancement of conductance is related to the fact that the spin precession reduces the angle between the accumulated spin and the magnetization direction of the drain electrode. This is even better illustrated in the lower panel of Fig. 3 which shows the same curves but normalized to conductance at parallel magnetization ($\theta = 0$). For $\epsilon/k_B T = -3$, the conductance stays almost flat over a broad range, and then establishes the spin-valve effect only in a small region around $\theta = \pi$.

Finally, we comment that a finite spin-flip relaxation time τ_{sf} will reduce the spin-valve effect and limit its observability to $\Gamma > \tau_{sf}^{-1}$ [17]. The main prediction of our theory, the deviation from the $\cos\theta$ -law, will not be

affected by τ_{sf} , as long as a θ -dependence is visible.

To summarize, there are two pronounced features in the linear conductance which proves the spin precession proposed in this Letter: (i) the shift of two adjacent conductance peaks towards each other with increasing angle θ (Fig. 2), and (ii) strong deviation from the $\cos\theta$ law for the spin-valve effect (Fig. 3).

Acknowledgements. – We thank G. Schön, J. Barnaś, and S. Maekawa for discussion. This work was supported by the Deutsche Forschungsgemeinschaft under the Center for Functional Nanostructures and the Emmy-Noether program.

-
- [1] M. Jullière, Phys. Lett. A **54**, 225 (1975).
 - [2] J. C. Slonczewski, Phys. Rev. B **39**, 6995 (1989).
 - [3] J. S. Moodera and L. R. Kinder, J. Appl. Phys. **79**, 4724 (1996); H. Jaffrès *et al.*, Phys. Rev. B **64**, 064427 (2001).
 - [4] K. Ono, H. Shimada, and Y. Ootuka, J. Phys. Soc. Jpn. **66**, 1261 (1997).
 - [5] J. Barnaś and A. Fert, Phys. Rev. Lett. **80**, 1058 (1998); S. Takahashi and S. Maekawa, Phys. Rev. Lett. **80**, 1758 (1998); A. Brataas, Yu. V. Nazarov, J. Inoue, and G. E. W. Bauer, Phys. Rev. B **59**, 93 (1999); J. Barnaś *et al.*, Phys. Rev. B **62**, 12363 (2000); J. Martinek *et al.*, Phys. Rev. B **66**, 014402 (2002).
 - [6] W. Rudziński and J. Barnaś, Phys. Rev. B **64**, 085318 (2001); G. Usaj and H. U. Baranger, Phys. Rev. B **63**, 184418 (2001); J. Martinek, Y. Utsumi, H. Imamura, J. Barnas, S. Maekawa, J. König, and G. Schön, cond-mat/0210006.
 - [7] Y. Chye *et al.*, Phys. Rev. B **66**, 201301(R) (2002); M. M. Deshmukh and D. C. Ralph, cond-mat/0207333.
 - [8] Y. Manassen *et al.*, Phys. Rev. Lett. **62**, 2531 (1989); C. Durkan and M. E. Welland, Appl. Phys. Lett. **80**, 458 (2002).
 - [9] D. Mozyrsky *et al.*, Phys. Rev. B **66**, 161313 (2002); Jian-Xin Zhu and A. V. Balatsky, cond-mat/0206191; L. N. Bulaevskii, M. Hruška, and G. Ortiz, cond-mat/0212049.
 - [10] R. Jansen and J. S. Moodera, Appl. Phys. Lett. **75**, 400 (1999); S. Tanoue and A. Yamasaki, J. Appl. Phys. **88**, 4764 (2000).
 - [11] J. König and Y. Gefen, Phys. Rev. Lett. **86**, 3855 (2001).
 - [12] J. König and Y. Gefen, Phys. Rev. B **65**, 045316 (2002).
 - [13] B. Kubala and J. König, Phys. Rev. B **65**, 245301 (2002).
 - [14] J. König, H. Schoeller, and G. Schön, Phys. Rev. Lett. **76**, 1715 (1996); J. König, J. Schmid, H. Schoeller, and G. Schön, Phys. Rev. B **54**, 16820 (1996); H. Schoeller, in *Mesoscopic Electron Transport*, edited by L. L. Sohn, L. P. Kouwenhoven, and G. Schön (Kluwer, Dordrecht, 1997); J. König, *Quantum Fluctuations in the Single-Electron Transistor* (Shaker, Aachen, 1999).
 - [15] This equation is the same as Eq. (4.4) of Ref. 12 but with the dot labels 1 and 2 replaced by \downarrow and \uparrow , and with no additional spin index to be summed over.
 - [16] In equilibrium and for lowest order, the finite magnetization in the leads does not yield a spin accumulation in the dot. To understand this let us first include a finite density of states for minority spins in the leads. Then, majority-spin electrons enter the QD at a higher rate

than minority spins but this is exactly compensated for by a higher rate for the majority spin to leave the dot. This remains true also in the half-metallic limit.

[17] Spin-flip relaxation times up to several μs have been ob-

served in GaAs quantum dots, T. Fujisawa, Y. Tokura, and Y. Hirayama, Phys. Rev. B **63**, 081304(R) (2001).